MAPPING COMPOSITIONAL DIVERSITY ON MARS: SPATIAL DISTRIBUTION AND GEOLOGICAL IMPLICATIONS. Sara Martínez-Alonso[1], Michael T. Mellon[1], Bruce M. Jakosky[1,2], and Bruce C. Kindel[3]. [1]Laboratory for Atmospheric and Space Physics, University of Colorado Boulder, 392 UCB, Boulder CO 80309-0392 (martinas@lasp.colorado.edu). [2]Department of Geological Sciences, University of Colorado Boulder. [3]Program in Atmospheric and Oceanic Sciences, University of Colorado Boulder.

Introduction: Visible and infrared spectrometers of high spatial resolution (e.g., Mars Express OMEGA, Mars Reconnaissance Orbiter CRISM) on board Mars orbiting missions will allow for detailed surface composition mapping of critical regions, necessary for the identification of future landing sites. Determining from existing global datasets the critical regions to be surveyed in detail with such instruments is essential to optimize the scientific return of those missions. The Spectral Variance Index (SVI) method [1, 2, 3, 4] identifies, from statistical analysis of the Mars Global Surveyor Thermal Emission Spectrometer (TES) global dataset [5], regions on the surface of Mars characterized by higher-than-average spectral variance, and therefore dominated by the presence of diverse materials, rather than by a spectrally homogeneous cover.

Many relevant geological processes coincide resulting in the concentration of a large diversity of surface materials (minerals, lithologies) in small regions. As an example, terrestrial hydrothermal systems are characterized by the presence of a wide variety of mineral species in relatively small geographical areas; because each mineral species has a distinct spectral signature, this translates into higher-than-average variance in the spectral remote sensing data of hydrothermal areas [6, 7]. Other geological processes that produce/concentrate a large variety of surface materials are: chemical sedimentation (such as water-laid deposition of carbonates and evaporites, characterized by layering of diverse composition), clastic sedimentation (such as in glacial and fluvial systems), pyroclastic volcanism, erosion unveiling layering, and differential weathering (chemical, mechanical), among others. Understanding those processes is of great importance to understanding the geological, hydrological, and (potentially) exobiological history of Mars: sedimentary deposits and weathering (or lack thereof) would be indicative of past and present climatic and hydrological regimes; hydrothermal and water-laid deposits would be prime sites to look for chemical and biological signatures of past and present life on Mars. Here we present a global SVI map and we discuss its significance by comparison to martian landers observations and to other global maps.

Spectral Variance Index Calculation: The SVI quantifies the amount of spectral variance present in the TES emissivity data per surface unit. The spectral variance per band measures, in a set of spectra, the average departure in emissivity from the band's mean. The spectral variance is the sum of the spectral variances calculated for all the spectral bands considered, and is equal to the sum of their eigenvalues. If all the spectra in the dataset have similar properties, both in the location and amplitude of their emissivity minima and maxima (that is, if all the spectra correspond to the same material), then their spectral variance will be low. Conversely, if the dataset contains different types of spectra (from different materials), its spectral variance will be higher. To calculate the global SVI values, daytime TES emissivity single-scan spectra were collected for 5-by-5 degree cells covering the entire planet, and filtered according to several quality criteria: no spatial or spectral averaging, close-to-nadir acquisition geometry, low atmospheric dust and ice opacities, brightness temperatures ≥250 K for maximum signal to noise, and instrument performance; noisy data and data with the signature characteristic of elevated amounts of atmospheric water vapor were also identified and discarded. The TES emissivity spectra gathered for each cell were then processed applying a principal components-like transformation used to segregate noise from the data and to reduce the computational requirements. The spectral variance per cell was computed by adding up the resulting eigenvalues above 3 standard deviations of the noise. As expected, there is a positive linear correlation between spectral variance and number of spectra per cell; the SVI is expressed as number of standard deviations of the residuals between observed and expected (from the linear correlation) spectral variance per cell. The global distribution of SVI values is shown in figure 1.A.

Discussion: *In situ* data from the five martian landing sites corroborate the SVI results. Viking Lander 1 (22.5°N, 48°W), Viking Lander 2 (48°N, 225.7°W), Pathfinder (19.3°N, 33.5°W), and Mars Exploration Rover Spirit (14.6°S, 184.5°W) landed in similar, monotonous regions dominated by fine materials and fragments of dark rocks [8, 9, 10] identified in the last two sites as basaltic-andesite and basaltic, respectively. This is consistent with the very low SVI values of those landing regions (-1.2, 0.5, -0.4, and –0.3, respectively). The Mars Exploration Rover Opportunity (1.9°S, 5.5°W) landed on a cell of elevated SVI (2.7); this is consistent with the complex mineralogy/lithology of the region: hematite, olivine, jarosite, and other sulfates have been identified as constituents of the fine materials and rocks (basaltic and sedimentary) present in the

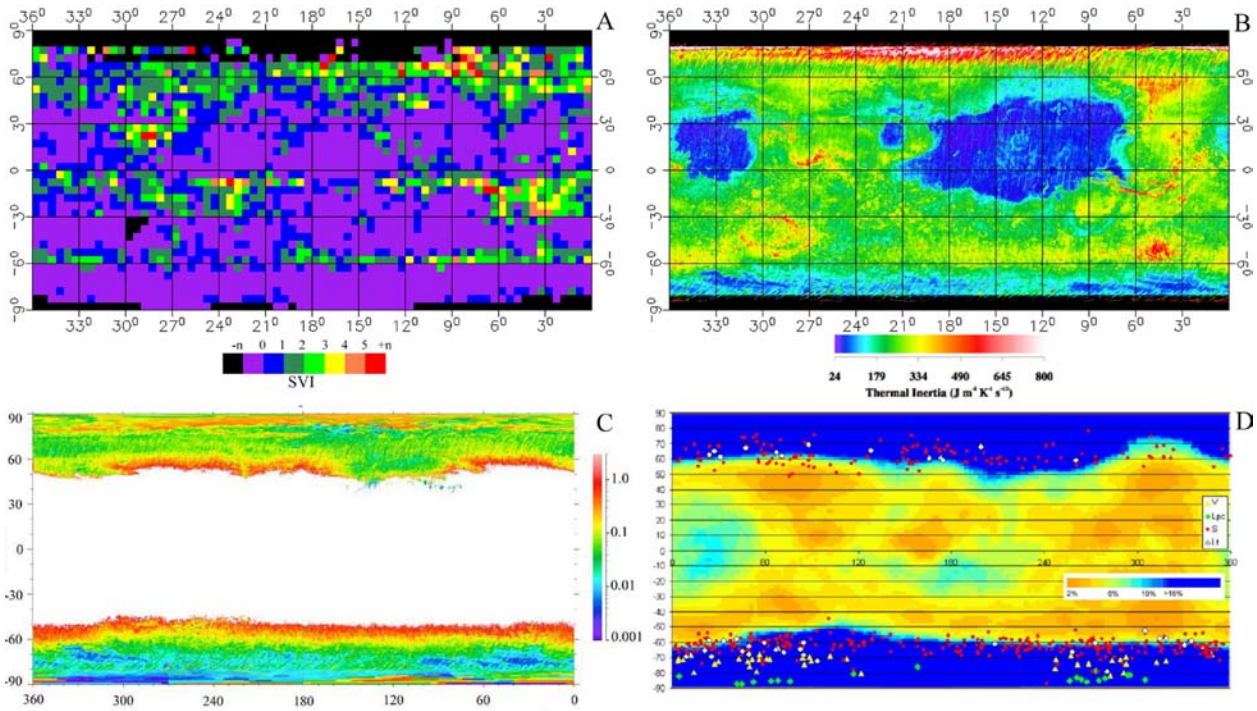

Figure 1. A: Spectral Variance Index map [4]. **B:** TES-derived thermal inertia map, modified from [14]. **C:** Calculated depth in m of the ice table, modified from [15]; white indicates regions of ground-ice instability. **D:** Red circles indicate distribution of small (<40 m) homogeneous polygons overlaid to ground ice proportion map, from [16].

landing area [11].

The global SVI map provides a complementary view of surface spectral properties, depicting the degree of diversity of exposed materials. It has remarkable spatial coherence and is broadly comparable to other global maps. SVI and albedo [12] present an approximate inverse correlation: high SVI regions coincide with low albedo areas, indicative of exposed rocky material; low SVI regions with high albedo areas, interpreted as dust-covered. The SVI distribution presents a rough positive correlation with thermal inertia [13, 14] (figure 1.B). Very low SVI values (≤1) dominate in vast low thermal inertia regions, commonly interpreted as mostly covered by dust, and therefore spectrally bland. Anomalously high SVI values (≥3) occur in high thermal inertia regions, interpreted as surfaces dominated by rocks. Some high SVI regions coincide with previously known regions of higher-than-average mineralogical/lithological diversity (e.g., Nili Fossae, Valles Marineris); others were not previously known [2, 4]. The SVI map shows latitudinal bands of relatively high values near 60°N and 60°S. These high SVI bands coincide with bands of high thermal inertia and low albedo. They are in close proximity to the subsurface ice stability boundary [15] (figure 1.C) and to regions characterized by the presence of small (<40 m), homogeneous polygons [16] (figure 1.D), similar to terrestrial ice wedge polygons. The high SVI bands also coincide with the pole-ward limits of dissected mantled terrains [17, 18], disaggregating deposits cemented by ice. These observations suggest that the high SVI latitudinal bands may be the compositional surface expression of climate-related processes previously recognized through morphological features. Ongoing analysis of the spectral, thermophysical, and morphological properties of high SVI regions will contribute to the clarification of their geological significance.

References: [1] Martínez-Alonso S. (2002) *Astrobiology Sc. Conf.*, 246. [2] Martínez-Alonso S. et al. (2002) *Astrobiology, 2*, 519. [3] Martínez-Alonso S. et al. (2003) *LPS XXXIV*, Abstract #1805. [4] Martínez-Alonso S. et al. (2004) *Manuscript in preparation*. [5] Christensen P.R. et al. (1992) *JGR, 97*, 7719-7734. [6] Boardman J.W. and Green R.O. (2000) *9th JPL Airborne Earth Sc. Worksho*p, 55-64. [7] Green R.O. and Boardman J.W. (2000) *9th JPL Airborne Earth Sc. Workshop*, 195-206. [8] Arvidson R.E. et al. (1989) *Rev. of Geophysics, 27*, 39-60. [9] Golombek M.P. et al. (1997) *Science, 278*, 1743-1748. [10] Squyres S.W. et al. (2004) *Science, 305*, 794-799. [11] Squyres S.W. et al. (2004) *Science, 306*, 1698-1703. [12] Pelkey S.M. and Jakosky B.M. (2002) *Icarus, 160*, 228-257. [13] Mellon M.T. et al. (2000) *Icarus, 148*, 437-455. [14] Putzig N.E. et al. (2004) *Icarus, in press*. [15] Mellon M.T. et al. (2004) *Icarus, 169*, 324-340. [16] Mangold N. et al. (2004) *JGR, 109*, E08001. [17] Mustard J.F. et al. (2001) *Nature, 412*, 411-414. [18] Head J.W. et al. (2003) *Nature, 426*, 797-802.